

On the Mechanism and Detection of Porosity During Pulsed TIG Welding of Aluminum Alloys

Yiming Huang, Zhifeng Zhang, Na Lv and Shanben Chen

Abstract Porosity is the remarkable barrier to realize the high efficient automatic welding of aluminum alloy. The paper provides new insights into the nucleation mechanism of porosity formation during pulsed TIG welding of aluminum alloys. Firstly, the model of bubble's nucleation based on inclusions is proposed. The calculated pore minimum radius shows large sensitivity to pulse duty cycle as well as welding current. Then a novel method based on spectral analysis to detect porosity is developed. The relationships among the extracted signals and porosity deflection are discussed, and the results show that Ar and HI spectral lines can be used as an aid to determine the most likely position of the porosity.

1 Introduction

Aluminum alloy is widely used to make low density and high strength structures in aerospace, military-industrial sectors due to its high comprehensive mechanical properties and good conductive heat conduction [1, 2]. These structures are of great significance, which require higher welding quality. But as a result of big thermal expansion coefficient, strong oxidizing, easy to inhale, a weld is inclined to deformation, crack, oxidation as well as porosity. And porosity is most likely to occur among those common defects in aluminum alloy welding process [3, 4], the morphology and distribution of which is one of the important factors that affect the material performance and microstructure.

Porosity widely exists in all kinds of welding methods, including MIG welding, laser welding, TIG welding and so on. Therefore, in the past several decades the study of porosity has been the hot spot in welding researches.

Y. Huang · Z. Zhang · N. Lv · S. Chen (✉)

Intelligentized Robotic Welding Technology Laboratory, School of Materials Science and Engineering, Shanghai Jiao Tong University, Shanghai, People's Republic of China
e-mail: sbchen@sjtu.edu.cn

Haboudou et al. [5] studied the influence of mechanical surface preparation as well as dual spot on porosity formation during Nd:YAG laser welding of A356 and AA5083 aluminum alloys. It is recognized that cleanliness of base metal is extremely important for reaching aluminum sound welds. Matsunawa et al. [6] found the type of shielding gas employed in high power CW CO₂ laser welding causes large differences in penetration and the formation of porosity defects. That is to say, the penetration depth of base metal is the deepest and a number of characteristic pores are formed with an inert shielding gas. Morais [7] evaluated the influence of different GMAW metal transfer modes on porosity generation in an AA5052 alloy using the gravimetric method. He concluded that pulsed GMAW leads to lesser porosity than welds carried out with the standard transfer modes. Da Silva and Scotti [8] proposed that the double pulsed GMAW technique does not increase the porosity susceptibility in aluminum welding in spite of having theoretically higher potential for porosity generation.

As to the detection of porosity, the main methods are acoustic emission testing and radiographic inspection. Aboali et al. [9] and Tao et al. [10] respectively determined several kinds of weld deflections, including lack of penetration, porosity and slag, by using acoustic emission testing technology. The results show that the distribution range of AE parameter value caused by porosity is bigger, but the amount of AE signals caused by welding porosity and other defects is roughly in the same order of magnitude. Sun et al. [11] and Valavanis and Kosmopoulos [12] respectively presented a method based on real-time X-ray image for detecting and discriminating discontinuities that may correspond to false alarms or defects such as porosity, linear slag inclusion, gas pores, lack of fusion or crack. However, the detection methods mentioned above both have some limitations. The result of ultrasonic testing is often judged by experience; X-ray inspection has a higher requirement to equipment. So it urgently needs a new NDT technology which can quickly inspect inside porosity deflection.

The key to reduce porosity lies in understanding the mechanism of the porosity formation and how the welding parameters affect the forming of porosity quantitatively. However, the researches on the mechanism are relatively few. Seto et al. [13] explored the influence of keyhole and pulse on porosity formation, but the reason is expounded.

The objective of this work is to explore the mechanism of porosity initial formation during pulsed TIG welding of aluminum alloys and to discuss the relationship between porosity and spectrum signals.

2 Porosity Formation Mechanism

As the initial stage of solidification of welding pool, bubble nucleation determines the distribution and size of pores, especially the minimum size of porosity. Therefore, factors influencing on porosity can be found by studying the bubble nucleation.

2.1 Nucleation Model

Liquid metal solidification of welding molten pool is similar to casting solidification process. But it has some unique characteristics, which consist of small size, fast cooling speed, solidifying with the moving heat source. Solidification of welding molten pool starts from the boundary to weld center in columnar crystal form. In view of the fact that cooling speed of aluminum alloy is very fast, non-equilibrium crystallizing process happens. Hydrogen precipitated during the welding process is not likely to be diffused evenly to the molten pool but to attach to high melting point inclusions. In the molten pool bubble heterogeneous nucleation is facilitated by inclusions, such as Al_2O_3 high melting point oxide, which reduced resistance of bubble nucleation because of its not wetting or partially wetting.

It is assumed that nucleation is conducted on the plane surface of inclusions, schematic diagram shown in Fig. 1.

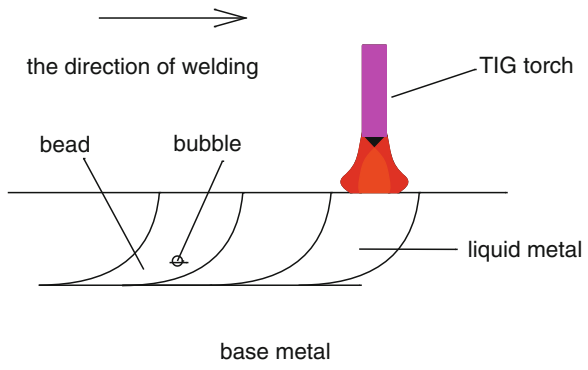
2.2 Theoretical Calculations

Bubble is presumed to be spherical with radius R . The Gibbs free energy ΔG of whole system is composed of two parts, including the reduction of volume free energy $-4\pi R^3 \Delta G_v / 3$ and the increment of interfacial free energy $4\pi R^2 \sigma_{LG}$ (Fig. 2). ΔG_v is described to be the work by draining away per unit volume of liquid metal. Therefore, formula (1) is obtained:

$$\Delta G = 4\pi R^2 \sigma_{LG} - \frac{4}{3} \pi R^3 P_b \tag{1}$$

According to Henry’s law, the gas-liquid interface keeps thermal dynamic equilibrium. When in balance state, in consideration of capillary pressure and arc force, relationship between internal pressure and external pressure of bubble can be gotten as formula (2):

Fig. 1 Schematic of nucleation based on the plane surface of inclusions



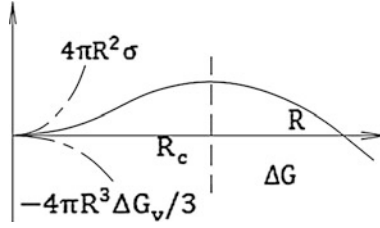


Fig. 2 Relationship between bubble radius and ΔG

$$P_b = P_{at} + P_s + P_C + P_{ar} \quad (2)$$

The static pressure of the bubble from the melt:

$$P_s = \rho_{al} \cdot g \cdot h \quad (3)$$

ρ_{al} is 2400 kg/m³, g is 9.8 N/kg, h is considered to be constant (3 mm) in contrast to the height of base metal (5 mm).

As it's known that capillary pressure is caused by surface tension, so

$$\begin{aligned} P_C dV &= \sigma_{LG} dS \\ P_C &= \frac{2\sigma_{LG}}{R} \end{aligned} \quad (4)$$

P_{ar} is caused by arc force, which consists of electromagnetic force, plasma flow force and gas evaporation force. However, the last force is usually neglected because it is far smaller than the first two forces. Therefore, it is expressed as formula (5).

$$P_{ar} = \frac{F_e + F_p}{S} \quad (5)$$

It is presumed that the projection on the pool is approximate to a circle with radius R_b , R_a is regarded as the radius of tungsten electrode.

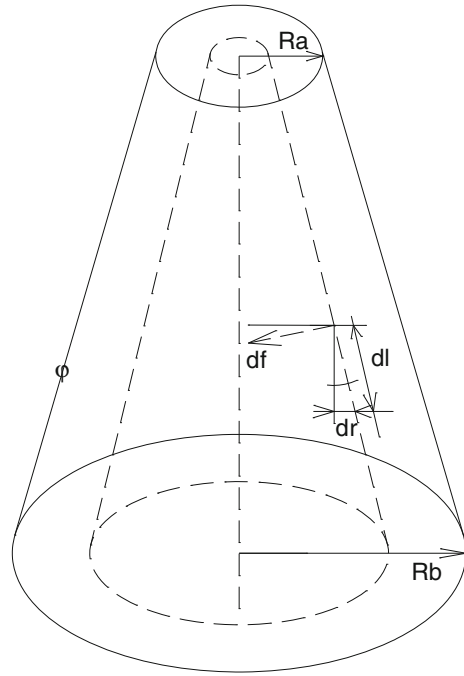
$$S = \pi R_b^2 \quad (6)$$

The arc shape is simplified to circular truncated cone, as shown in Fig. 3. And the assumption is made that current I goes evenly through each section of the arc. Therefore, magnetic induction intensity is B

$$B = \mu_0 H = \frac{\mu_0 i}{2\pi r_i} \quad (7)$$

i is the current going through the circle with radius r_i .

Fig. 3 Schematic diagram of simplified arc shape



The component of electromagnetic force per unit length dl in the direction from tungsten electrode to the molten pool is df_{\perp} , with the following expression:

$$df_{\perp} = \sin \varphi \cdot df = \frac{dr}{dl} \cdot B \cdot di \cdot dl = \frac{\mu_0 i di dr_i}{2\pi r_i} \tag{8}$$

The integration of df_{\perp} in radial direction:

$$dF = \int_{R_a}^{R_b} df_{\perp} = \frac{\mu_0 i di}{2\pi} \ln \frac{R_b}{R_a} \tag{9}$$

Then F_e is obtained by integrating dF :

$$F_e = \int_0^I dF = \frac{\mu_0 I^2}{4\pi} \ln \frac{R_b}{R_a} \tag{10}$$

For TIG welding, when arc length is more than 2 mm, radial distribution of plasma flow force is in concordance with the hyperbolic curve. That is to say:

$$f_p = F_{\max} \exp(-a|r|) \tag{11}$$

F_{\max} is arc force in central axis, proportional to the square of the current; a is concentration factor of the distribution curve as well as constant; r is the radial coordinate value

$$F_p = \int_0^{2\pi} \int_0^{R_b} \frac{1}{2r} f_p dr d\theta = \frac{\pi a^2 F_{\max}}{2R_b^2} \int_0^{R_b} \frac{r^3 e^{-ar} dr}{1 - e^{-ar}(1 + ar)} \quad (12)$$

$$F_{\max} = \varepsilon I^2 \quad (13)$$

ε is proportionality coefficient as well as constant.

Alternating current pulse TIG welding process is chosen in the experiment, T_p and T_b are period of peak value and base value current respectively.

$$I = \begin{cases} I_p n(T_p + T_b) \leq t \leq n(T_p + T_b) + T_p \\ I_b n(T_p + T_b) + T_p \leq t \leq (n+1)(T_p + T_b) \end{cases} \quad (14)$$

From the classical solidification nucleation theory, it's known that the maximum of ΔG corresponds to the critical embryo.

$$\frac{D(\Delta G)}{dR} = 8\pi R \sigma_{LG} - 4\pi R^2 P_b - \frac{4}{3} \pi R^3 \frac{dP_b}{dR} = 0 \Big|_{R=R_c} \quad (15)$$

By solving the above equation set, the critical radius of bubble is obtained as following expression:

$$R_o = \frac{2\sigma_{LG}}{3(P_{at} + \rho_{al}gh + P_{ar})}$$

When current is equal to base value I_b , $R_b = 1.5R_a$

$$P_{ar} = \frac{F_e + F_p}{S} = \frac{1}{\pi R_b^2} \left[\frac{\mu_0 I_b^2}{4\pi} \ln \frac{R_b}{R_a} + \frac{\pi \varepsilon a^2 I_b^2}{2R_b^2} \int_0^{R_b} \frac{r^3 e^{-ar} dr}{1 - e^{-ar}(1 + ar)} \right]$$

When current is equal to peak value I_p , $R_b = 3R_a$

$$P_{ar} = \frac{F_e + F_p}{S} = \frac{1}{\pi R_b^2} \left[\frac{\mu_0 I_p^2}{4\pi} \ln \frac{R_b}{R_a} + \frac{\pi \varepsilon a^2 I_p^2}{2R_b^2} \int_0^{R_b} \frac{r^3 e^{-ar} dr}{1 - e^{-ar}(1 + ar)} \right]$$

3 Results and Discussions

3.1 Experimental System

The diagram of the experimental system is shown in Fig. 4, which consists of two subsystems. The welding subsystem is worked with an OTC INVERTER ELESON 500P-type TIG welding power, a fixed water-cooled gas tungsten arc (GTA) torch. The data collection subsystem can obtain image, sound and spectrum information. The latter is studied in our research and acquired by a 3648 linear CCD spectrometer HR4000 UV-NIR, with spectral resolution of 0.02 nm (FWHM). Table 1 shows the chemical compositions (wt%) of 5A06 aluminum alloy and ER5183 welding wire.

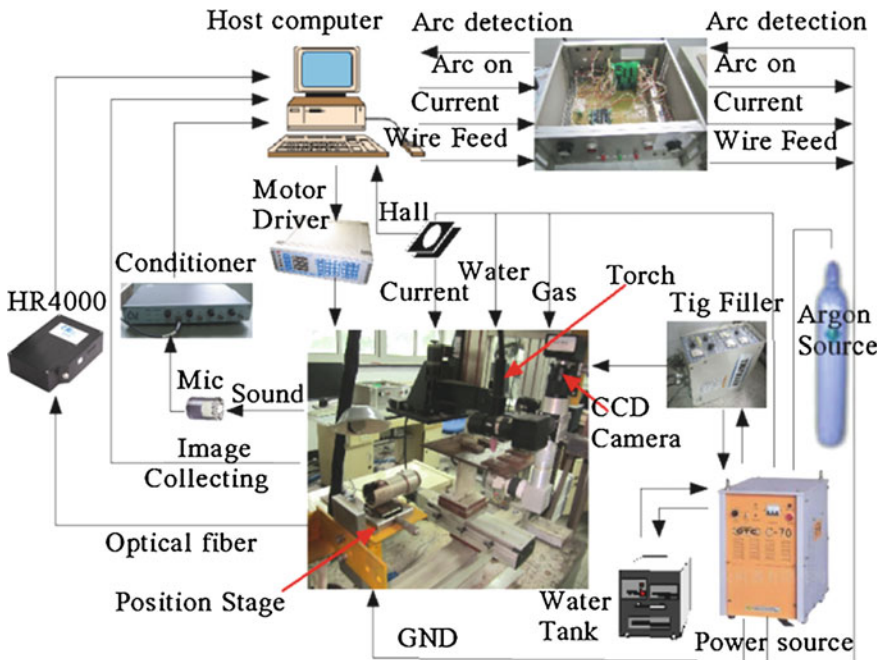


Fig. 4 Schematic diagram of the experiment system

Table 1 Chemical compositions of 5A06 Al alloy

Element	Mg	Mn	Fe	Si	Zn	Cu	Al
5A06	5.8–6.8	0.5–0.8	≤0.4	≤0.4	≤0.2	≤0.1	Bal.
ER5183	4.3–5.2	0.5–1.0	0.4	0.4	0.25	0.1	Bal.

A commercial 5A06 sheet was sheared into sample sizes of $260 \times 50 \times 4 \text{ mm}^3$. 99.999 % pure argon gas with a flow rate of 12 L/min was selected as the shielding gas. In order to remove oxide film on the surface of the aluminum alloy, reduce the loss of tungsten electrode, control energy, experiments of 5A06 aluminum alloy are done by AC pulse TIG welding method. Through the test, the welding parameter is gotten shown in Table 2.

Table 2 Normal welding parameters

Pulse frequency (Hz)	Peak current (A)	Base current (A)	Welding speed (mm/s)	Electrode diameter (mm)	Ar flow (L/min)	Pulse duty ratio (%)
1	170	50	3	3.2	12	50

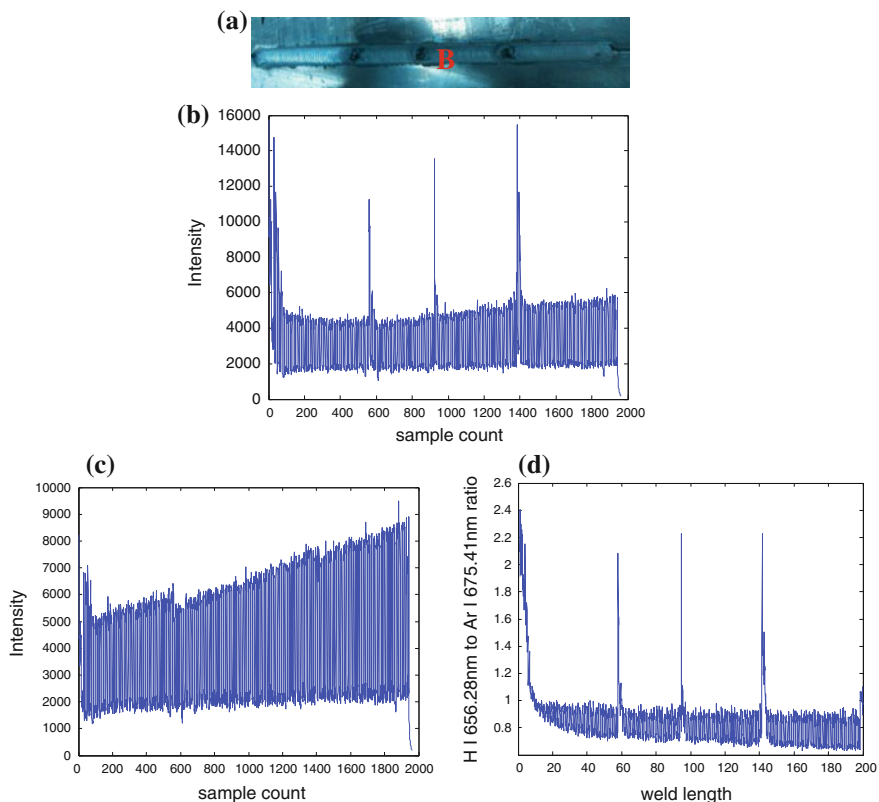


Fig. 5 a Welding seam, b intensity of HI 656.28 nm, c intensity of Ar I 675.41 nm, d ratio of HI 656.28 nm and Ar I 675.41 nm

3.2 Detection of Porosity Based on Spectral Analysis

Under normal atmospheric pressure, hydrogen partial pressure of arc atmosphere is determined by hydrogen content of arc atmosphere. Hydrogen of arc atmosphere generates radiation spectrum under the effect of electric arc heat, and the content of hydrogen is positively related to the intensity of the spectrum. Given that hydrogen of arc atmosphere is in dynamic equilibrium with hydrogen in the molten pool, the detection of porosity can be achieved by the measurement of hydrogen spectral intensity.

To obtain apparent porosity deflection, artificial boreholes are made and hydrocarbons are added in Fig. 5a. The spectral signals of HI 656.28 nm and Ar I 675.41 nm are collected by spectrometer, shown in Fig. 5b, c. It's obvious that the intensity of spectrum line becomes greater and greater through the welding process. And the intensity of HI 656.28 nm has a steep rise in the position where deflection happens, while Ar I 675.41 nm is completely on the contrary to HI 656.28 nm. To eliminate the effect of welding heat input on the intensity of H spectrum line and avoid wrong judgment, the ratio of intensity of HI 656.28 nm and Ar I 675.41 nm is used to determine the deflection.

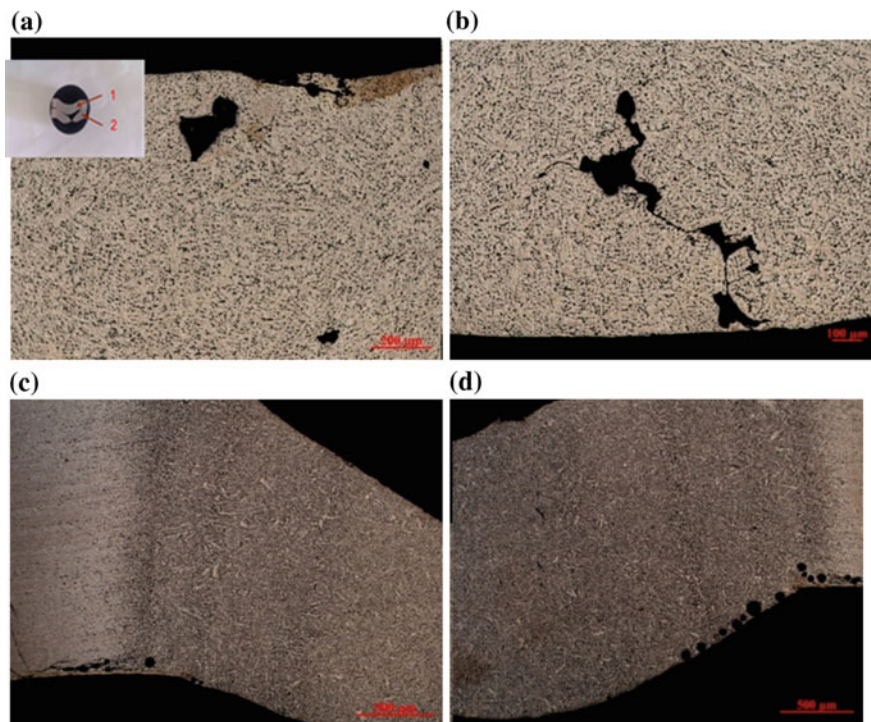


Fig. 6 a The upper of section 1, b the bottom of section 1, c the left side of section 2, d the right side of section 2

3.3 Observation of Internal Surfaces of Porosity

Transaction is selected along the vertical welding direction of specimen from the welding deflection B (shown in Fig. 5a) every 2 mm. Microstructure and morphology are investigated by means of the optical microscopy, shown in Fig. 6. The upper of section 1 exists several porosity deflections, one of which is bigger because of the combination of multiple holes. There is crack deflection in the bottom of the welding seam. And pores distribute intensively in the both left and right sides of the root in section 2.

4 Conclusions

The principal conclusions obtained from this study may be summarized as follows:

1. New insights into the nucleation mechanism of porosity formation during pulsed TIG welding of aluminum alloys are proposed. As parameters are constant or in accordance with specific welding conditions, the relationship between critical radius and current is acquired by theoretical deduction. The critical radius can be regarded as the minimum radius of porosity, which shows large sensitivity to pulse duty cycle as well as welding current.
2. The content of hydrogen in the arc atmosphere can be monitored by H spectrum line. To eliminate the effect of welding heat input on the intensity of H spectrum line and avoid wrong judgment, the ratio of intensity of H I 656.28 nm and Ar I 675.41 nm is used to determine the content of hydrogen. It indicates serious porosity deflection when the ratio is greater than 1.

Acknowledgment This work is supported by the National Natural Science Foundation of China under the Grant No. 61401275

References

1. Liu G, Sun J, Nan CW et al (2005) Experiment and multiscale modeling of the coupled influence of constituents and precipitates on the ductile fracture of heat-treatable aluminum alloys. *Acta Mater* 53(12):3459–3468
2. Nanninga N, White C, Furu T et al (2008) Effect of orientation and extrusion welds on the fatigue life of an Al–Mg–Si–Mn alloy. *Int J Fatigue* 30(9):1569–1578
3. Malin V (1991) Efficient welding fabrication of extruded aluminum mat panels. ELECTROCOM GARD NILES IL
4. Mathers G (2002) *The welding of aluminium and its alloys*. Woodhead publishing, Cambridge
5. Haboudou A, Peyre P, Vannes AB et al (2003) Reduction of porosity content generated during Nd: YAG laser welding of A356 and AA5083 aluminum alloys. *Mater Sci Eng A* 363(1):40–52

6. Matsunawa A, Mizutani M, Katayama S et al (2003) Porosity formation mechanism and its prevention in laser welding. *Weld Int* 17(6):431–437
7. Morais FC (2001) Influence of operational factors on porosity formation in aluminum MIG welding. Federal University of Uberlandia, Brazil
8. Da Silva CLM, Scotti A (2006) The influence of double pulse on porosity formation in aluminum GMAW. *J Mater Process Technol* 171(3):366–372
9. Aboali A, El-Shaib M, Sharara A et al (2014) Screening for welding defects using acoustic emission technique. *Adv Mater Res* 1025:7–12
10. Tao Y, Wang W, Sun B (2014) Nondestructive online detection of welding defects in track crane boom using acoustic emission technique. *Adv Mech Eng* 2014
11. Sun Y, Bai P, Sun H et al (2005) Real-time automatic detection of weld defects in steel pipe. *NDT & E Int* 38(7):522–528
12. Valavanis I, Kosmopoulos D (2010) Multiclass defect detection and classification in weld radiographic images using geometric and texture features. *Expert Syst Appl* 37(12):7606–7614
13. Seto N, Katayama S, Matsunawa A (2001) Porosity formation mechanism and suppression procedure in laser welding of aluminum alloys. *Weld Int* 15(3):191–202